Uncoupled numerical method for fracture analysis

J.C.W. VAN VROONHOVEN[1] and R. DE BORST[2,3]

[1] *Philips Research Laboratories, Prof. Holstlaan 4, 5656 AA Eindhoven, The Netherlands*
[2] *Eindhoven University of Technology, Faculty of Mechanical Engineering, P.O. Box 513, 5600 MB Eindhoven, The Netherlands*
[3] *Delft University of Technology, Faculty of Civil Engineering, P.O. Box 5048, 2600 GA Delft, The Netherlands*

Abstract. An uncoupled numerical method for the analysis of dynamic crack propagation is proposed. The approach consists of two main steps. Firstly, the internal stresses in the intact, unfractured, elastic body are calculated with the use of the finite element method. In this calculation it is assumed that no cracks are present and that fracture does not occur. Secondly, a theoretical crack is initiated and possible crack paths are derived from the elastic stress data. The stress-intensity factors for the planar fracture modes I and II, for the anti-plane mode III, and for the bending modes 1 and 2 are calculated from the well-known, linearized expressions for arbitrary, slightly curved cracks in thin plate-like and shell-like structures. The direction and speed of crack propagation are determined from a dynamic fracture criterion based on the energy release rate. Several applications of the uncoupled numerical method are presented, concerning standard fracture specimens loaded by tensile forces and bending moments, a single-edge notched beam loaded by shear forces, and a three-dimensional cylindrical tube loaded by torsional moments. Good agreement with both experimental and numerical results from the literature has been obtained. The major advantages of the uncoupled approach are its ease-of-use and the limited computational effort.

Key words: cracks, dynamics, failure, finite element analysis, fracture mechanics.

1. Introduction

For a practical analysis of the structural integrity of complex mechanical structures, it is necessary to obtain good insight in the distribution of the internal stresses. Such analyses typically consist of the following stages

(i) a calculation of the elastostatic stresses in the intact, unfractured structure due to constant external loads;

(ii) a calculation of the elastodynamic stresses in the intact, unfractured structure due to time-dependent external loads;

(iii) a calculation of the initial, quasi-static propagation of cracks in the fractured structure due to constant external loads; and

(iv) a calculation of the prolonged, dynamic propagation of cracks in the fractured structure due to constant or time-dependent external loads.

These stages are of increasing difficulty. The finite element method has proved to be an efficient means for the elastic stress calculations mentioned under (i) and (ii); see Hughes [1] and Zienkiewicz [2]. Special crack-tip elements have been developed for the calculation of the crack propagation mentioned under (iii) and (iv). These elements incorporate the stress singularity at the crack tip, either by interpolation of the displacements with the use of square-root functions (Stern and Becker [3, 4]) or by application of quarter-point nodes on the element sides adjacent to the crack tip (Barsoum [5]).

A strong disadvantage occurs in the application of the finite element method to the calculations mentioned under (iv). Namely, dynamic fracture involves both stress waves and crack propagation. These dynamic effects interact: the stresses determine the crack propagation, while rapid fracture initiates new stress waves. This interaction can only be incorporated in a fully-coupled dynamic fracture analysis. In addition, the material rupture and the creation of new crack surfaces lead to a continuous change in the geometry of the structure. This necessitates a continuous adaptation of the element mesh, a shift of the special crack-tip elements to the new position of the crack tip, and a transfer of variables from the old to the new element division. An overview of computational studies on dynamic crack propagation, including moving finite element techniques, is presented by Nishioka, Murakami and Takemoto [6]. In such studies the crack path is often assumed to be straight or otherwise to be known beforehand. When the crack propagates along an arbitrary, a priori unknown, curved path, many finite elements must be adapted. Since these adaptations require much computing time, a fully-coupled dynamic fracture analysis is time-consuming and therefore often unsuitable for a practical study of dynamic crack propagation in large mechanical structures.

As an alternative approach, we propose an uncoupled numerical fracture method (see van Vroonhoven [7, 8]) based on the calculation of the elastodynamic stresses for the intact configuration. The response of the intact structure due to constant or time-dependent external loads is determined with the use of the finite element method and standard finite elements. It is assumed that the material remains linearly elastic and that fracture does not occur. Afterwards, as a form of post-processing, predictions of crack paths are computed from the elastic stress data. The interaction between the crack propagation and the stress waves as described above has only partially been accounted for in this uncoupled method, because the effect of the crack propagation on the stress distribution is neglected. Also, the mutual influence of multiple cracks is not incorporated. Of course, it cannot be expected that this uncoupled numerical method will produce results with utmost precision for the entire fracture process, especially near the moment of final collapse. Nevertheless, it is possible to analyse the initial phases of crack propagation with reasonable accuracy.

The great benefit of the uncoupled numerical fracture method is that a fixed finite element division is sufficient and that mesh adaptation is not necessary. In addition, several independent crack paths can be determined from one elastodynamic stress calculation. This implies a considerable reduction of computing time in comparison with a fully-coupled dynamic fracture analysis where each crack path must be determined in a separate dynamic calculation. Since the direction of crack propagation immediately after the onset of fracture is mostly of crucial importance for the overall safety of the structure [7, Chapter 1], it is often sufficient to study only the first moments of crack propagation. This corresponds precisely to the range of validity of the uncoupled numerical fracture method. Therefore, we expect that the uncoupled method can produce useful results with a limited numerical effort.

2. Theory and numerical method

The uncoupled numerical fracture method has been developed for the analysis of fracture problems involving rapid crack propagation and/or dynamic loading conditions [7, 8]. Nevertheless, this method can also be used to examine quasi-static crack propagation in structures under constant loads. There is one restriction: the uncoupled method applies to thin, slightly curved, plate-like or shell-like structures and is less suitable for analyzing general crack propagation in thick three-dimensional solids. This restriction is related to the manner of crack

representation, which is described below. We shall now give a detailed description of the uncoupled numerical fracture method which consists of four distinct steps.

2.1. ELASTIC STRESS CALCULATION

The first step of the uncoupled numerical fracture method is the determination of the stresses in the intact, unfractured, elastic body as a function of time, either analytically (if possible) or numerically by means of a finite element computation. In order to perform a dynamic analysis, it is necessary to calculate the initial equilibrium situation first. Most structures (for example test specimens) may initially be in a stress-free state, or subjected to gravitational forces, or in another simple stress situation. The elastodynamic calculation continues with the addition of the time-dependent external loads and the computation of the stresses for several time increments. Evidently, a quasi-static analysis can be carried out by taking the stresses constant in time and equal to the initial stress distribution.

2.2. CRACK INITIATION AND CRACK REPRESENTATION

The initiation of a crack is the second step of the uncoupled numerical fracture method. The precise location of crack initiation can be chosen freely, in combination with the initial length and orientation of the crack. For example, the location may be at the position of the highest stress, near a sharply rounded edge, or at a joint between different materials. It is also possible to choose an initiation location where the stresses attain a local maximum, a point where an external force is applied, or any other critical position in the structure.

Regarding the crack representation, we impose some restrictions on the geometry of the structure under investigation and on the shape of the crack surfaces. The structure is assumed to be a thin, flat plate or a thin-walled, slightly curved shell. Three-dimensional structures which do not have constant thickness and/or are not entirely flat, can also be analyzed and can be regarded as thin flat plates, as long as the thickness variations and the curvature remain relatively small. The shape of the crack is subject to the conditions that the crack front is assumed to be a straight line, and that the crack surfaces are assumed to be perpendicular to the middle plane of the plate. As a result, it is not possible to incorporate variations of the crack front over the thickness of the plate nor the degree of crack rotation. These latter effects may occur when the crack propagates at different speeds in the upper and lower surfaces of the plate or in different directions. In these cases, the crack front is no longer a straight line perpendicular to the middle plane of the plate, but will rotate and attain a skew orientation with respect to the plate normal. Observations on three-dimensional fractured specimens, however, indicate that the cracks are almost perpendicular to the plate surfaces in many cases.

The projection of the crack onto the middle plane of the plate is described by the crack-shape function $y = \lambda(x)$ with $-a \leqslant x \leqslant +a$. The coordinates x and y are the in-plane Cartesian coordinates, which are related to the crack geometry and chosen such that the two end points of the crack are on the x-axis. Thus, we have $\lambda(\pm a) = 0$; see also Figure 1. The perpendicular coordinate is denoted by z where $-h/2 \leq z \leq +h/2$. In the general situation, the plate thickness h may depend on x and y. Obviously, there exists a relation between these crack-related coordinates and the global Cartesian coordinates X, Y, Z which are used for the elastic stress calculation.
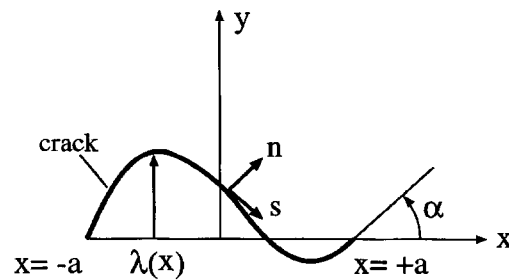
Figure 1. Geometry of an arbitrary curvilinear crack with crack-shape function $\lambda(x)$ and with normal and tangential directions n and s.
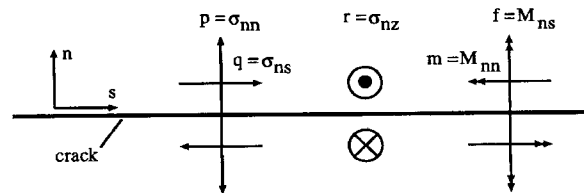

Figure 2. Various loading components acting on the crack surfaces, corresponding to the in-plane fracture modes I and II, the anti-plane fracture mode III, and the bending fracture modes 1 and 2.

2.3. STRESS-INTENSITY FACTORS

The third and fourth steps of the uncoupled numerical fracture method concern the determination of the crack path. After the crack initiation and at any moment of the crack-path calculation, both the speed and the direction of crack propagation must be computed. To this end, we use the expressions for the stress-intensity factors for curvilinear cracks in plates, which have been derived by Cotterell and Rice [9] and by van Vroonhoven [7, 10, 11]. We distinguish five different modes of fracture, namely the usual modes I and II of planar deformation and mode III of anti-plane deformation, plus two additional modes to describe the out-of-plane bending deformation. The bending modes are referred to by the arabic numerals 1 for normal bending and 2 for torsion; see van Vroonhoven [7, 11] and Hui and Zehnder [12].

The crack path is taken as a piece-wise linear curve with the sequential positions of the crack tip as its vertices and with the crack increments as the connecting lines. The crack-shape function $\lambda(x)$ is determined for each vertex by measurement of the distance to the line connecting the end points of the crack path (the x-axis). The stress distributions along the crack surfaces are derived from the elastic stresses which have been calculated at step one of the uncoupled method. The in-plane stresses on opposite crack surfaces are taken equal; only the perpendicular shear stresses on both crack surfaces are taken opposite. The stress components along the crack in the positions $(x, \lambda(x), z)$ are denoted by $\sigma_{ij}(x, z)$ with $-a \leqslant x \leqslant +a$ and $-h/2 \leqslant z \leqslant +h/2$. The directions normal and tangential to the crack surfaces are denoted by n and s, respectively, as illustrated in Figures 1 and 2.

The stress-intensity factors K_I and K_{II} for the opening and sliding modes (planar deformation) have been derived in [9] by a perturbation analysis and a linearization procedure with respect to the crack-shape function $\lambda(x)$. The results obtained by this analysis are expressed

in terms of the averaged normal and tangential stresses on the crack surfaces (see also Figure 2):

$$p(x) = \frac{1}{h(x)} \int_{-h(x)/2}^{+h(x)/2} \sigma_{nn}(x,z)\,\mathrm{d}z = \frac{1}{2} \int_{-1}^{+1} \sigma_{nn}(x,\zeta h(x)/2)\,\mathrm{d}\zeta, \tag{1}$$

$$q(x) = \frac{1}{h(x)} \int_{-h(x)/2}^{+h(x)/2} \sigma_{ns}(x,z)\,\mathrm{d}z = \frac{1}{2} \int_{-1}^{+1} \sigma_{ns}(x,\zeta h(x)/2)\,\mathrm{d}\zeta, \tag{2}$$

where $\zeta = 2z/h(x)$ is the dimensionless thickness coordinate. The linearized results for the stress-intensity factors are then given by

$$K_{\mathrm{I}} = \frac{1}{\sqrt{\pi a}} \int_{-a}^{+a} [p(x) + (\lambda'(x) - \tfrac{3}{2}\alpha)q(x)] \left(\frac{a+x}{a-x}\right)^{1/2}\,\mathrm{d}x$$

$$- \frac{1}{\sqrt{\pi a}} \int_{-a}^{+a} \frac{a\lambda(x)q(x)}{(a+x)^{1/2}(a-x)^{3/2}}\,\mathrm{d}x, \tag{3}$$

$$K_{\mathrm{II}} = \frac{1}{\sqrt{\pi a}} \int_{-a}^{+a} [q(x) - (\lambda'(x) - \tfrac{1}{2}\alpha)p(x)] \left(\frac{a+x}{a-x}\right)^{1/2}\,\mathrm{d}x$$

$$- \frac{1}{\sqrt{\pi a}} \int_{-a}^{+a} \frac{a\lambda(x)p(x)}{(a+x)^{1/2}(a-x)^{3/2}}\,\mathrm{d}x, \tag{4}$$

where α is the inclination angle at the right crack tip: $\tan\alpha = \lambda'(a)$.

The stress-intensity factor K_{III} for the tearing mode (anti-plane shear) has been calculated in [7, Section 5.2] and [10]. It has been shown that the linearized result is independent of the crack-shape function $\lambda(x)$, and that the function $\lambda(x)$ is only present in the expression for K_{III} in the case of asymmetric loading of the crack, that is, when the perpendicular shear stresses on the two crack surfaces are not precisely opposite. The reasons for the dissimilarity with the expressions for K_{I} and K_{II} are twofold [7, Section 5.4]. Firstly, two independent fracture modes (I and II) exist in the case of planar deformation, whereas only one fracture mode (III) exists in the case of anti-plane shear. Secondly, the stress-intensity factors K_{I} and K_{II} are expressed in terms of tensile and shear stresses in the directions normal and tangential to the crack surfaces; these directions are related to the derivative $\lambda'(x)$ of the crack-shape function. The factor K_{III}, on the contrary, is expressed in terms of shear stresses acting in the z-direction; this direction is constant along the crack. Thus, K_{III} depends on the derivative $\lambda'(x)$ to a lesser extent than the other two factors. The linearized expression for K_{III} is given by

$$K_{\mathrm{III}} = \frac{1}{\sqrt{\pi a}} \int_{-a}^{+a} r(x) \left(\frac{a+x}{a-x}\right)^{1/2}\,\mathrm{d}x, \tag{5}$$

where the function $r(x)$ indicates the averaged perpendicular shear stress:

$$r(x) = \frac{1}{h(x)} \int_{-h(x)/2}^{+h(x)/2} \sigma_{nz}(x,z)\,\mathrm{d}z = \frac{1}{2} \int_{-1}^{+1} \sigma_{nz}(x,\zeta h(x)/2)\,\mathrm{d}\zeta. \tag{6}$$

The stress-intensity factors k_1 and k_2 for the normal bending and torsional modes have been calculated in [7, Section 5.3] and [11] on the basis of Kirchhoff's classical plate theory. For details on this plate theory we refer to the textbooks by Timoshenko and Woinowsky-Krieger [13] and Savin [14, Chapter VI]. The analysis in [7, 11] utilizes similar linearization and perturbation techniques as in [9]. The stress-intensity factors are expressed in terms of the (integrated) normal bending moments $m(x)$ and torsional moments $f(x)$ per unit length; see Figure 2. These cross-sectional quantities are expressed in Nm/m and are defined by

$$m(x) = \int_{-h(x)/2}^{+h(x)/2} \sigma_{nn}(x,z)z \, dz = \tfrac{1}{4}h^2(x) \int_{-1}^{+1} \sigma_{nn}(x,\zeta h(x)/2)\zeta \, d\zeta, \tag{7}$$

$$f(x) = \int_{-h(x)/2}^{+h(x)/2} \sigma_{ns}(x,z)z \, dz = \tfrac{1}{4}h^2(x) \int_{-1}^{+1} \sigma_{ns}(x,\zeta h(x)/2)\zeta \, d\zeta. \tag{8}$$

The linearized results for the bending stress-intensity factors are given by

$$k_1 = \frac{6}{\sqrt{\pi a}} \int_{-a}^{+a} g_1(x) \left(\frac{a+x}{a-x}\right)^{1/2} dx - \frac{6}{\kappa\sqrt{\pi a}} \int_{-a}^{+a} \frac{a\lambda(x)f(x)}{(a+x)^{1/2}(a-x)^{3/2}} dx, \tag{9}$$

$$k_2 = \frac{6}{\sqrt{\pi a}} \int_{-a}^{+a} g_2(x) \left(\frac{a+x}{a-x}\right)^{1/2} dx - \frac{6}{\kappa\sqrt{\pi a}} \int_{-a}^{+a} \frac{(2x-a)\lambda(x)m(x)}{(a+x)^{1/2}(a-x)^{3/2}} dx$$

$$+ \frac{12(\kappa+1)}{\kappa(\pi a)^{3/2}} \int_{-a}^{+a} m(x)\sqrt{a^2-x^2} \int_{-a}^{+a} \frac{\lambda(s)}{\sqrt{a^2-s^2}(x-s)} ds \, dx, \tag{10}$$

where $\kappa = -(3+\nu)/(1-\nu)$ with ν being the Poisson's ratio of the material. The integrand functions $g_1(x)$ and $g_2(x)$ are defined by

$$g_1(x) = \frac{m(x)}{h^2(x)} + \left(\lambda'(x) - \frac{\kappa+1}{\kappa}\mathcal{A} + \left(\frac{\kappa+1}{\kappa}\mathcal{A} - \frac{2\kappa+1}{2\kappa}\alpha\right)\left(\frac{2x-a}{a}\right)\right)\frac{f(x)}{h^2(x)}, \tag{11}$$

$$g_2(x) = \left(\frac{2\kappa-1}{2\kappa}\alpha - \frac{2\lambda(x)}{\kappa a} - \lambda'(x)\left(\frac{2x-a}{a}\right)\right)\frac{m(x)}{h^2(x)} + \left(\frac{2x-a}{a}\right)\frac{f(x)}{h^2(x)}, \tag{12}$$

where the dimensionless crack-shape parameter $\mathcal{A}$ is defined by

$$\mathcal{A} = \frac{1}{\pi a} \int_{-a}^{+a} \lambda'(x)\left(\frac{a+x}{a-x}\right)^{1/2} dx. \tag{13}$$

The last term in (10) contains a double integral in which the inner, singular integral must be calculated by taking the Cauchy principal value. Interchanging the order of integration is allowed [7, 11]. We note that the expressions for k_1 and k_2 are more complicated than those for K_I and K_{II} due to the constant κ and the factor $(2x-a)/a$. Equating this constant to unity and disregarding this factor in (9)–(12) results in simplified expressions for k_1 and k_2, which resemble the expressions (3) and (4) of planar deformation [7, 11].

2.4. CRACK PROPAGATION

For the calculation of the crack-propagation direction and speed, we use the fracture criterion based on the energy release rate or the J-integrals; see Broek [15, Chapter 5], Cherepanov

[16, Chapter 5] and Freund [17]. According to van Vroonhoven [7, Chapter 4] and Hui and Zehnder [12], the integral J_1 for mixed-mode fracture is given by

$$J_1 = \frac{h}{E}(K_I^2 + K_{II}^2) + \frac{h}{2G}K_{III}^2 + \frac{h(1+\nu)}{3E(3+\nu)}(k_1^2 + k_2^2), \tag{14}$$

where h is the plate thickness in the crack-tip region, E is the Young's modulus, ν is the Poisson's ratio, and $G = E/2(1 + \nu)$ is the shear modulus of the material. Because of the thin, plate-like geometry, it is assumed that conditions of plane stress apply. The integral J_1 is related to the amount of energy dissipation per unit length of crack advance and is expressed in J/m. As an alternative to the factors k_1 and k_2 of the classical plate theory, the stress-intensity factors K_1 and K_2 of Reissner's plate bending theory [18, 19] can be used. The relation between k_1 and k_2 on one hand and K_1 and K_2 on the other hand is given by [7, 12]

$$\frac{k_1}{K_1} = \frac{k_2}{K_2} = \left(\frac{3+\nu}{1+\nu}\right)^{1/2}, \tag{15}$$

so that the integral J_1 can be expressed as

$$J_1 = \frac{h}{E}(K_I^2 + K_{II}^2) + \frac{h}{2G}K_{III}^2 + \frac{h}{3E}(K_1^2 + K_2^2). \tag{16}$$

The integral J_2 in Reissner's theory has been calculated in [7, Chapter 4] and is equal to

$$J_2 = -\frac{2h}{E}K_I K_{II} - \frac{2h}{3E}K_1 K_2. \tag{17}$$

The direction of crack propagation is now derived from the vector **J** with component J_1 in the direction ahead of the crack and with component J_2 in the perpendicular direction in the plane of the plate. Following Cherepanov [16, Chapter 5], we take the direction of this vector **J** as the direction of crack propagation. The angle θ_p with respect to the current direction of the crack is then determined by

$$\tan \theta_p = \frac{J_2}{J_1}. \tag{18}$$

The speed of crack propagation is derived from a dynamic fracture criterion based on the theories of Freund [17]. We denote the energy release rate for a dynamically propagating crack by $\mathcal{G}(\sigma, a, c)$ where σ represents the stress state or the externally applied forces, a is the crack length, and $c = \dot{a}$ is the crack speed. It has been shown in [17, Chapter 6] that the dynamic energy release rate for a propagating crack is equal to the energy release rate $\mathcal{G}(\sigma, a, 0)$ for the static equilibrium state of a stationary crack of the same size a and subjected to the same external load σ, multiplied by a universal function of the crack speed c, viz.

$$\mathcal{G}(\sigma, a, c) = g(c)\mathcal{G}(\sigma, a, 0), \tag{19}$$

where $g(c)$ is the universal function of crack speed. An accurate approximation of this function is (see [7, Section 3.5] and [17])

$$g(c) = (1 - c/c_R)\sqrt{1 - c/c_d}, \tag{20}$$

where $0 \leqslant c \leqslant c_R < c_d$ with c_R and c_d being the speeds of Rayleigh waves and dilatational waves, respectively. Since the relations (16)–(17) are valid for crack propagation under quasi-static conditions, we take the length of the vector **J** as the energy release rate for the static equilibrium situation [16, Chapter 5]. Thus, we obtain the expression

$$\mathcal{G}(\sigma, a, 0) = \sqrt{J_1^2 + J_2^2}. \tag{21}$$

The crack speed c is now determined by putting the dynamic energy release rate $\mathcal{G}(\sigma, a, c)$ in (19) equal to the critical energy release rate $\mathcal{G}_c$ which is a material constant.

During the numerical computation, the new position of the crack tip is calculated from

$$\mathbf{x}_{tip,\,new} = \mathbf{x}_{tip,\,old} + \mathbf{c} \cdot \Delta t_c, \tag{22}$$

where Δt_c is the time step for the crack-propagation increment and **c** is a vector in the plane tangent to the plate with length equal to the crack speed c and with its direction determined by the crack-propagation angle θ_p. It is emphasized that the time step Δt_c for the fracture simulation may be larger than the time step used in the finite element computation of the elastodynamic stresses. However, the time step Δt_c cannot be chosen too large because otherwise the numerical accuracy of the crack path will be insufficient. In situations with static loading conditions, we may use a crack increment Δx with fixed length and with its direction determined by the angle θ_p as given in (18). The latter procedure is equivalent to putting the crack speed c equal to a fixed value, for instance the Rayleigh wave speed c_R, and choosing an appropriate time step Δt_c.

After the determination of the new crack-tip position, the third and fourth steps in the uncoupled numerical fracture method are repeated. The stress-intensity factors for the new, extended crack are calculated and, as long as the resulting value of $\mathcal{G}(\sigma, a, 0)$ exceeds the critical energy release rate $\mathcal{G}_c$, the crack propagation will continue. It is assumed that the dynamic fracture process remains unstable (see [16, Chapter 4] and [17, Chapter 1]). But when $\mathcal{G}(\sigma, a, 0)$ decreases and becomes less than $\mathcal{G}_c$, the crack-propagation speed c becomes zero and crack arrest occurs.

Finally, we emphasize that the uncoupled numerical fracture method admits the analysis of only one crack at a time. It is possible to analyze the propagation of multiple cracks by performing separate, parallel computations on the basis of the procedure described above. Every crack calculation starts with the initiation of a new crack, which may be chosen at a different position and with a different initial length and/or orientation. The ease-of-use of the uncoupled method becomes apparent when we consider the significant numerical effort involved in a (dynamic) finite element computation compared to the relatively small amount of post-processing for uncoupled fracture simulations. The elastic stress calculation for a large, complicated geometry can be quite elaborate and can require several hours of computing time. But such stress calculation for the intact geometry always has to be performed in a practical failure analysis. Namely, it is one of the simplest ways to obtain insight in the internal stress distributions, as we have mentioned in the introduction where these calculations were referred to as stages (i) and (ii). The time needed to calculate a crack path by the uncoupled method ranges from a few minutes to at most one hour on a HP-9000 computer, depending on the length of crack extension. The fully-coupled fracture calculations of stages (iii) and (iv), on the other hand, need an amount of computing time which is normally considerably larger than that for the elastodynamic stress calculation for the intact geometry. The advantages of the

uncoupled numerical fracture method are obvious: the elastodynamic stress data are already available and can be used again for repeated, uncoupled crack-path calculations, resulting in large savings in computing time.

3. Discussion of uncoupled calculation

The uncoupled numerical fracture method uses elastic stress data of the unfractured configuration to make crack-path predictions. This may sound contradictory, but it can be explained by the following argument for quasi-static fracture. In the first step of an uncoupled analysis, we compute the elastic stress distribution for the intact structure under the assumption that fracture does not occur. In the next steps, we *assume* the existence of a crack at a certain position and at a given moment of time. This crack, however, is a theoretical crack in the sense that it does not exist in reality. The stresses in these positions are considered to act on the crack surfaces, opening the crack, and creating a stress singularity at its tip. This leads to a paradox, since there are no singularities in the computed stress data. On the other hand, the surfaces of a real crack would have been stress-free. This paradox is explained with the superposition principle (see Broek [15, Section 3.5]) for the situation of a mode I crack.

Consider the intact, unfractured, elastic body loaded by prescribed external forces. The distribution of the internal stresses is calculated at step one of the uncoupled method. Also consider three related configurations under different loading conditions illustrated in Figure 3. Firstly, the body (a) contains a crack with stress-free crack surfaces and is subjected to the same external loads as the intact, unfractured, elastic body. Due to the presence of the crack, stress relief occurs resulting in crack opening. Secondly, the body (b) having the same geometry as (a) is loaded by extra stresses $\sigma_{nn} = p(x)$ being applied to the crack surfaces in the direction n normal to the crack. These stresses tend to close the crack and the function $p(x)$ is chosen such that complete crack closure occurs and that the stress singularities at the crack tips vanish. Because of the disappearing stress singularities, the configuration (b) coincides with the intact, unfractured geometry. The difference between (a) and (b) is obtained by subtraction. This results in configuration (c) where no externally applied forces are present; only the crack surfaces are subjected to stresses $\sigma_{nn} = -p(x)$ having opposite sign with respect to body (b). These stresses tend to open the crack and create stress singularities at the crack tips. Because of the superposition principle, the stress intensities for (a) and (c) are identical. The stress distribution $p(x)$ is derived from the solution of problem (b) or, equivalently, from the solution for the intact, unfractured, elastic body. The obtained stress distribution is then used for the calculation of the stress-intensity factors. This argument shows that the influence of the stress situation on the stress-intensity factors is correctly incorporated in the uncoupled numerical fracture method.

The argumentation presented above reveals some limitations of the uncoupled numerical fracture method, regarding the dynamic effects. As described in the introduction, the stresses and the crack propagation are linked. Firstly, the crack-path predictions are based on the elastic stress situation. This equally applies to dynamic and static fracture processes. Secondly, rapid crack propagation induces stress waves emanating from the moving crack tip and the continuous change in the geometry leads to different relations between the stresses and the external loads. The latter effect, i.e., the influence of the propagating crack on the stress field, is neglected in the uncoupled method. The dynamic interaction is only incorporated in the universal function of the crack speed $g(c)$ which relates the elastodynamic energy release rate to its static equivalent, as shown in the equation (19). Because of the partial incorporation of
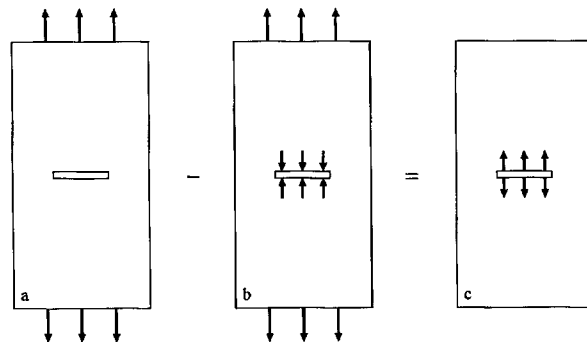
Figure 3. Three configurations illustrating the principle of superposition. Configuration (a) with external load and stress-free crack surfaces, minus configuration (b) with extra stresses closing the crack, is equivalent to configuration (c) with opposite stresses applied to the crack surfaces and without external load.

the dynamic effects, the uncoupled method can only produce reliable results for the initial phases of crack propagation, but not over the full range of the fracture process. This is not considered a major problem, since the initial phases of crack propagation are generally seen as the most important ones in judging the structural integrity of the constructions.

4. Numerical results and discussion

The uncoupled numerical fracture method has been incorporated, together with a finite element program, in the MATLAB programming environment [20]. For the division of the geometries into finite elements, the mesh generation program SEPMESH of the SEPRAN package [21] has been utilized. Since the uncoupled method is applied to thin-walled structures under tension and bending loads, the 8-node brick elements of Wilson and Taylor [22, 23] are employed; see also Hughes [1, Section 4.7] and MacNeal [24, Chapter 8]. These elements have eight corner nodes and additional, quadratic interpolation functions (or shape functions) to ensure the correct bending stiffness of the element. The additional interpolation functions are commonly called 'incompatible modes'. Standard 8-node brick elements with linear interpolation functions are unsuitable for the solution of general elasticity problems, since these elements cannot incorporate the quadratic displacements occurring in bending deformation. These standard linear elements appear to be too stiff. Furthermore, the Wilson–Taylor elements use a Gaussian quadrature rule with eight ($2 \times 2 \times 2$) integration points, which is more economic than the 20-node quadratic brick elements with either a 27-point ($3 \times 3 \times 3$) Gaussian quadrature rule or a 14-point non-Gaussian quadrature rule; see Irons [25]. This establishes a considerable reduction in computing time for the assembly process. Moreover, van Vroonhoven [7, Section 7.5] has shown that the elements of Wilson and Taylor give a far better performance concerning the calculation of the displacements and the stresses than some other 8-node brick elements, such as under-integrated elements.

4.1. SQUARE PLATE LOADED BY TENSILE FORCES OR BENDING MOMENTS

A series of numerical tests has been carried out to investigate the accuracy and the reliability of the uncoupled numerical fracture method. The first test concerns the possible dependence of the calculated crack path on the finite element division. To this end, we study a square plate
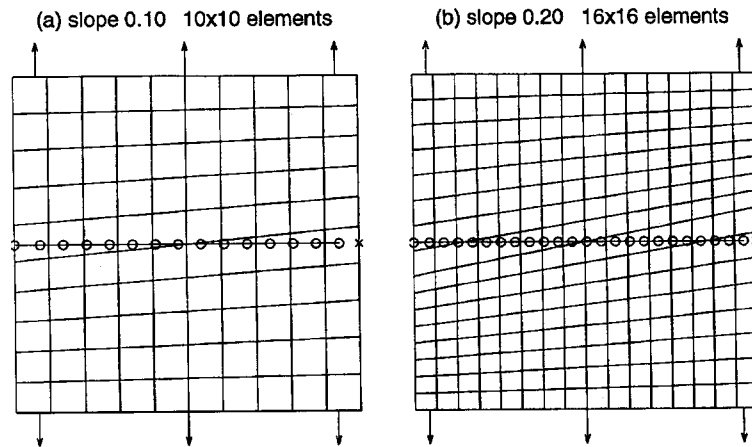
(a) slope 0.10   10x10 elements   (b) slope 0.20   16x16 elements

Figure 4. Crack paths in a square plate loaded by tensile forces, derived with the uncoupled numerical fracture method. Subsequent positions of the crack tip are shown by o and the prospective end point of the crack by ×.

of size $l \times l$ and thickness $h = l/20$, loaded by uniform tensile forces or uniform bending moments on two opposite sides. The plate is divided into $n \times n$ elements with one element over the thickness; the elements have a variable, slanted orientation. After the stress calculation a crack is initiated at the middle of one of the traction-free sides. A crack increment Δx of fixed length is used to simulate quasi-static crack propagation. The initial crack length is equal to 3/4 of the element width and the crack increments are chosen equal to 2/3 of the element width.

Calculations have been performed for various numbers of elements and for various different element orientations. In Figure 4 we show some typical results for the crack paths in the plate loaded by tensile forces, for (a) an element division with $n = 10$ and a maximum slope of the element lines equal to 0.10, and for (b) an element division with $n = 16$ and a maximum slope of 0.20. These slopes correspond to inclination angles of the mesh lines of 5.7° and 11.3°, respectively. Subsequent positions of the crack tip are marked by open circles. The prospective end point of the crack is at the middle of the traction-free side opposite to the point of crack initiation and is indicated by ×. Similar results have been obtained for the plate loaded by bending moments, where anti-clastic bending behaviour [13, Section 11] is observed in the displacement solution due to the applied moment. Because of the simple loading configuration, the fracture process can be described by one stress-intensity factor: K_I for the tension problem and k_1 (or K_1) for the bending problem. A trivial solution is obtained with a uniform uniaxial stress state and with a straight crack path, despite the slanted element orientation. Refinement of the element division and selection of other inclination angles also produce straight crack paths for both loading situations.

In order to illustrate that the crack speed is calculated correctly, we have also performed a dynamic uncoupled fracture analysis of the square plate under tensile forces, for the finite element division with $n = 16$ and a maximum slope of the element lines equal to 0.20. The Poisson's ratio ν has been set equal to 0.250, so that the Rayleigh wave speed equals $c_R = 0.5815\sqrt{E/\rho}$ with E the Young's modulus and ρ the density of the material. The initial crack length is again equal to 3/4 of the element width; the time step for the crack increment is chosen equal to $\Delta t_c = 0.090 \, l\sqrt{\rho/E}$. The resulting crack path is shown in Figure 5(a),
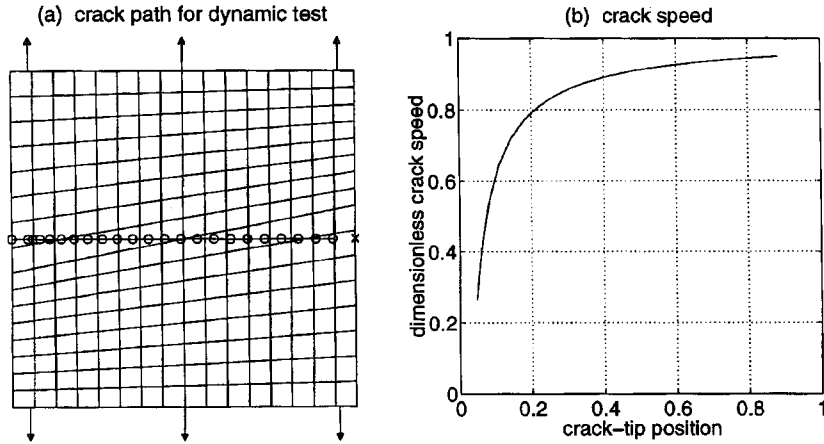
(a) crack path for dynamic test

(b) crack speed

Figure 5. Dynamic crack propagation: (a) crack path in a square plate loaded by tensile forces and (b) dimensionless crack speed c/c_R as function of the crack-tip position x_{tip}/l.

illustrating that the length of the crack increments gradually increases as the crack propagates. The crack speed as function of the crack-tip position is presented graphically in Figure 5(b) and is given by

$$c(x_{tip}) = c_R \cdot \left(1 - \frac{x_c}{x_{tip}}\right), \tag{23}$$

because the mode I stress-intensity factor is equal to $K_I = \sigma\sqrt{\pi x_{tip}}$ for a uniform stress field σ, as derived from (3). The result (23) coincides with the results obtained by Broek [15, Section 6.1]. The parameter x_c in (23) is the critical crack length and is derived from

$$K_c = \sqrt{E\mathcal{G}_c/h} = \sigma\sqrt{\pi x_c}. \tag{24}$$

When the initial crack length is smaller than x_c, no crack propagation will occur. Only cracks with an initial length larger than x_c will lead to fracture of the plate.

4.2. SINGLE-EDGE NOTCHED BEAM LOADED BY SHEAR FORCES

The next test concerns curvilinear crack propagation under shear loads. A suitable test for the examination of shear effects was proposed by Iosipescu [26], namely a beam with a single-edge notch loaded by compressive forces applied at four different points, as shown in Figure 6. We adopt the dimensions of Feenstra [27, Section 5.1] and Schlangen [28, Section 3.3] and study a beam of length 440 mm, height 100 mm, and thickness 10 mm. The forces F_1 are applied at a distance of 20 mm from the plane of symmetry and the forces F_2 at a distance of 200 mm. Because of mechanical equilibrium, we have $F_1 = 10F_2$. The beam is divided into a total of 264 elements with one element over the thickness and with refinement in the shear zone, where the elements are of size $10 \times 10 \times 10\,mm^3$.

A crack is initiated at the center of the long edge of the beam, in the plane of symmetry, with an initial length of (a) 15 mm or (b) 25 mm. The deformation of the beam is essentially two-dimensional and the fracture process can be described by a combination of the stress-intensity
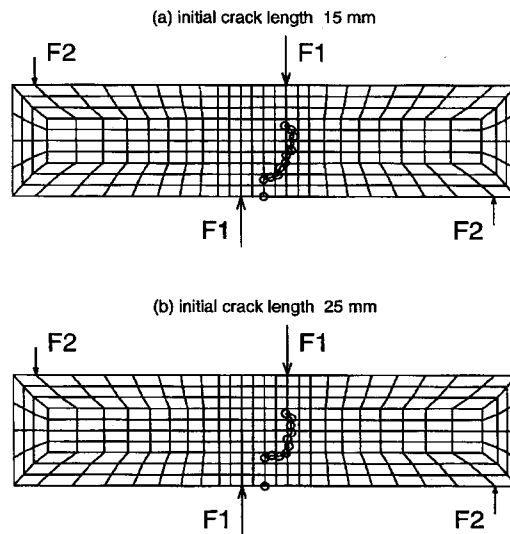
(a) initial crack length 15 mm

(b) initial crack length 25 mm

Figure 6. Crack paths in a single-edge notched beam loaded under shear conditions, derived with the uncoupled numerical fracture method. Subsequent positions of the crack tip are shown by o.

factors K_I and K_{II}. Due to the shear stresses, the crack propagation is (initially) dominated by mode II and will occur along a curved path ending on the opposite edge to the right of the point where the force F_1 is applied [28, Section 4.1]. The crack paths obtained with the uncoupled numerical fracture method, as shown in Figure 6, satisfy this requirement although deviations occur near the points of crack arrest. These deviations are caused by compressive stresses which occur in the uncoupled analysis. In a fully-coupled fracture analysis, these compressive stresses would shift to the top of the beam during crack propagation. The first part of the crack path is therefore reliable, while the second part must be considered with caution.

The crack paths of Figure 6 agree with both the experimental and the numerical results in [28, Sections 4.1, 6.2]. The present results are better than those in [27, Section 5.1] where a straight crack path inclined at an angle of approximately 45° with respect to the edge was obtained. Single-edge notched beams of other dimensions have been studied by Lubliner, Oliver, Oller and Oñate [29] with the use of a plastic-damage model and by Rots [30] with smeared and discrete crack representations. Their studies have led to similar results.

4.3. CYLINDRICAL PIPE LOADED BY TORSIONAL MOMENTS

A three-dimensional test problem with curvilinear crack propagation is the torsion of a hollow cylindrical pipe. The thickness of the pipe is 10 mm and the inner and outer radii are 30 and 40 mm. The pipe has a length of 400 mm and is loaded by torsional moments at both end surfaces. We choose a finite element division with 25 elements in the axial direction, 16 elements in the circular cross section, and one element over the thickness. Because of the torsional loading, a stress state of pure shear is obtained.

A crack is initiated in the middle cross section of the pipe and through the thickness. The initial crack length is 3/4 of the element size in the circumferential direction and the crack increments are 2/3 of that element size. The early stage of fracture is dominated by mode II,
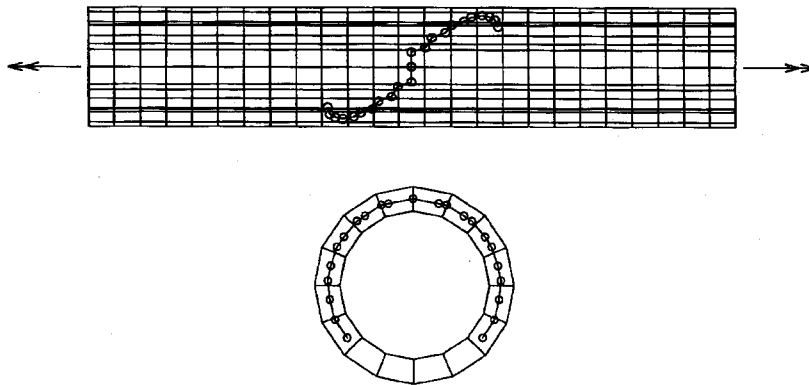
Figure 7. Crack paths in a cylindrical pipe loaded by torsional moments, derived with the uncoupled numerical fracture method. The initial crack is at the middle of the side view and at the top of the cross-sectional view. Subsequent positions of the crack tip (into two directions) are shown by o.

but the crack deflects in such a fashion that the stress-intensity factor K_I gradually becomes more dominant while K_{II} decreases. Crack propagation is determined in two (symmetric) directions and the pipe with the calculated crack paths is shown in Figure 7. The calculation is terminated when the linearized expressions (3)–(5) and (9)–(10) for the stress-intensity factors cannot be used anymore due to extreme curvature of the crack path. The present numerical results agree with the crack-path predictions based on the experimental work of Richard [31] and the theoretical work of Lakshminarayana and Murthy [32]. This example shows that the uncoupled numerical fracture method can also be used for a study of crack growth in shell-like structures.

5. Conclusions

Application of an uncoupled numerical fracture method to standard test problems has shown that this method is not susceptible to variations in the finite element division. This mesh independence concerns both the element size and the element orientation. In addition, applications to Iosipescu's single-edge notched shear beam and to the torsion of a cracked, hollow, cylindrical pipe have demonstrated that correct crack-propagation directions are derived for fracture under mixed-mode conditions and in three dimensions. The crack propagation was determined on the basis of the energy release rate in combination with the stress-intensity factors for arbitrary, slightly curved cracks. Moreover, the use of a dynamic fracture criterion enables the accurate calculation of the speed of crack propagation. Based on these considerations, we conclude that the uncoupled numerical fracture method produces trustworthy results, and that extension to more complicated problems is allowed.

Due to the partial uncoupling between crack propagation and dynamic effects, the results for prolonged crack propagation must be considered with caution, especially near the point of crack arrest or final collapse. Nevertheless, good crack-path predictions have been obtained for the early phases of fracture. The advantages of the uncoupled numerical fracture method are that adaptations of the finite element division are not necessary, and that the elastodynamic stress data can be used repeatedly for multiple crack computations. Thus, we conclude that

with this uncoupled method we have established an effective, powerful, and inexpensive tool for the analysis of crack propagation both in statically and in dynamically loaded structures.

Acknowledgements

References

1. T.J.R. Hughes, *The Finite Element Method.* Linear static and dynamic finite element analysis. Prentice-Hall, Englewood Cliffs NJ (1987).
2. O.C. Zienkiewicz, *The Finite Element Method.* McGraw-Hill, London (1977).
3. M. Stern, Families of consistent conforming elements with singular derivative fields. *International Journal for Numerical Methods in Engineering* 14 (1979) 409–421.
4. M. Stern and E.B. Becker, A conforming crack tip element with quadratic variation in the singular fields. *International Journal for Numerical Methods in Engineering* 12 (1978) 279–288.
5. R.S. Barsoum, On the use of isoparametric finite elements in linear fracture mechanics. *International Journal for Numerical Methods in Engineering* 10 (1976) 25–37.
6. T. Nishioka, R. Murakami and Y. Takemoto, The use of the dynamic J integral (J') in finite-element simulation of Mode I and mixed-mode dynamic crack propagation. *International Journal of Pressure Vessels and Piping* 44 (1990) 329–352.
7. J.C.W. van Vroonhoven, *Dynamic Crack Propagation in Brittle Materials: Analyses Based on Fracture and Damage Mechanics.* PhD Thesis, Eindhoven University of Technology, The Netherlands (1996).
8. J.C.W. van Vroonhoven, Uncoupled dynamic fracture approach. *Mechanisms and Mechanics of Damage and Failure, Proceedings of the 11th European Conference on Fracture ECF-11*, Poitiers, France (1996) 455–460.
9. B. Cotterell and J.R. Rice, Slightly curved or kinked cracks. *International Journal of Fracture* 16 (1980) 155–169.
10. J.C.W. van Vroonhoven, Stress intensity factors for curvilinear cracks loaded under anti-plane strain (mode III) conditions. *International Journal of Fracture* 70 (1995) 1–18.
11. J.C.W. van Vroonhoven, Stress intensity factors for curvilinear cracks loaded by bending and torsional moments. *International Journal of Fracture* 68 (1994) 193–218.
12. C.Y. Hui and A.T. Zehnder, A theory for the fracture of thin plates subjected to bending and twisting moments. *International Journal of Fracture* 61 (1993) 211–229.
13. S.P. Timoshenko and S. Woinowsky-Krieger, *Theory of Plates and Shells.* McGraw-Hill Kogakusha, Tokyo (1959).
14. G.N. Savin, *Stress Concentration around Holes.* Pergamon Press, Oxford (1961).
15. D. Broek, *Elementary Engineering Fracture Mechanics.* Kluwer Academic Publishers, Dordrecht, The Netherlands (1986).
16. G.P. Cherepanov, *Mechanics of Brittle Fracture.* McGraw-Hill, New York (1979).
17. L.B. Freund, *Dynamic Fracture Mechanics.* Cambridge University Press, Cambridge (1990).
18. E. Reissner, The effect of transverse shear deformation on the bending of elastic plates. *Transactions of ASME, Journal of Applied Mechanics* 12 (1945) A69–A77.
19. E. Reissner, On bending of elastic plates. *Quarterly of Applied Mathematics* 5 (1947) 55–68.
20. MATLAB, *High-Performance Numeric Computation and Visualization Software. Reference Guide.* The Math-Works, Natick MA (1992).
21. SEPRAN, *Sepra Analysis. Users Guide and Programmers Manual.* Ingenieursbureau Sepra, Leidschendam, The Netherlands (1993).
22. E.L. Wilson, R.L. Taylor, W.P. Doherty and J. Ghaboussi, Incompatible displacement models. *Numerical and Computer Methods in Structural Mechanics*, S.J. Fenves et al. (eds.), Academic Press, New York (1973) 43–57.
23. R.L. Taylor, P.J. Beresford and E.L. Wilson, A non-conforming element for stress analysis. *International Journal for Numerical Methods in Engineering* 10 (1976) 1211–1219.
24. R.H. MacNeal, *Finite Elements: Their Design and Performance.* Marcel Dekker, New York (1994).

25.   B.M. Irons, Quadrature rules for brick based finite elements. *International Journal for Numerical Methods in Engineering* 3 (1971) 293–294.

26.   N. Iosipescu, New accurate procedure for single shear testing of metals. *Journal of Materials* 2 (1967) 537–566.

27.   P.H. Feenstra, *Computational Aspects of Biaxial Stress in Plain and Reinforced Concrete*. PhD Thesis, Delft University of Technology (1993).

28.   E. Schlangen, *Experimental and Numerical Analysis of Fracture Processes in Concrete*. PhD Thesis, Delft University of Technology (1993).

29.   J. Lubliner, J. Oliver, S. Oller and E. Oñate, A plastic-damage model for concrete. *International Journal of Solids and Structures* 25 (1989) 299–326.

30.   J.G. Rots, Smeared and discrete representations of localized fracture. *International Journal of Fracture* 51 (1991) 45–59.

31.   H.A. Richard, Safety estimation for construction units with cracks under complex loading. *Structural Failure, Product Reliability and Technical Insurance*, H.P. Rossmanith (ed.), Inderscience Enterprises, Geneva (1987) 423–437.

32.   H.V. Lakshminarayana and M.V.V. Murthy, On stresses around an arbitrarily oriented crack in a cylindrical shell. *International Journal of Fracture* 12 (1976) 547–566.